Mechanisms for the enhancement of the thermal stability of organic thin films by aluminum oxide capping layers

S. Sellner
Max-Planck-Institut für Metallforschung, 70569 Stuttgart, Germany; and Institut für Theoretische und Angewandte Physik, Universität Stuttgart, 70550 Stuttgart, Germany

A. Gerlach[a] and F. Schreiber[b]
Physical and Theoretical Chemistry Laboratory, Oxford University, Oxford OX1 3QZ, United Kingdom

M. Kelsch
Max-Planck-Institut für Metallforschung, 70569 Stuttgart, Germany

N. Kasper
Max-Planck-Institut für Metallforschung, 70569 Stuttgart, Germany; and ANKA, FZ Karlsruhe, 76344 Eggenstein-Leopoldshafen, Germany

H. Dosch
Max-Planck-Institut für Metallforschung, 70569 Stuttgart, Germany; and Institut für Theoretische und Angewandte Physik, Universität Stuttgart, 70550 Stuttgart, Germany

S. Meyer and J. Pflaum
III. Physikalisches Institut, Universität Stuttgart, 70550 Stuttgart, Germany

M. Fischer and B. Gompf
I. Physikalisches Institut, Universität Stuttgart, 70550 Stuttgart, Germany

G. Ulbricht
Max-Planck-Institut für Festkörperforschung, 70569 Stuttgart, Germany

(Received 4 July 2005; accepted 31 October 2005)

We present a detailed study of the thermal stability of organic thin films of diindenoperylene encapsulated by sputtered aluminum oxide layers. We studied the influence of capping layer thickness, stoichiometry, and heating rate on the thermal stability of capped films and their eventual breakdown. Under optimized encapsulation conditions (thick and stoichiometric capping layer), the organic films desorb only at temperatures 200 °C above the desorption of the uncapped film. Moreover, the capped organic films retain their crystalline order at these elevated temperatures, whereas they would normally (i.e., uncapped) be in the gas phase. This study therefore also shows a way of studying organic materials under temperature conditions normally inaccessible. Considering results from complementary techniques, we discuss possible scenarios for the eventual breakdown. The results have implications for the performance and long-term stability of organic devices for which stability against elevated temperatures as well as against exposure to ambient gases is crucial.

I. INTRODUCTION

In recent years, great progress has been made in the area of organic semiconductor devices.[1–5] Such devices eventually have to meet certain stability requirements to find their way into commercial products. Exposure of the active organic films to ambient gases may cause gas penetration into the organic film and lead to oxidation or unintentional doping of the active transport layer.[6–8] Stability against elevated temperatures is important to guarantee a good long-term performance of such devices.[9–16] An obvious way of protecting the active layer against these degradation and failure mechanisms is encapsulation.[17]

Aluminum oxide is frequently used in device and coating technology due to its specific physical and chemical properties.[18,19] Sputtered aluminum oxide layers were used to encapsulate organic semiconductor films of

[a]Present address: Institut für Angewandte Physik, Universität Tübingen, Auf der Morgenstelle 10, 72076 Tübingen, Germany.
[b]Address all correspondence to this author.
Present address: Institut für Angewandte Physik, Universität Tübingen, Auf der Morgenstelle 10, 72076 Tübingen, Germany.
e-mail: frank.schreiber@uni-tuebingen.de
DOI: 10.1557/JMR.2006.0052

diindenoperylene (DIP) and to study the thermal stability of these systems. From electrical and structural measurements it was concluded that DIP is a good candidate for the application in organic devices.[20,21] In a previously published short communication, we reported the observation that capped films of DIP remain crystalline even at temperatures more than 200 °C above the desorption temperature of uncapped films.[22] On the basis of further experimental work, the present paper presents a detailed study of the underlying effects and responsible mechanisms of this remarkable enhancement.

Because the structure and morphology of the aluminum oxide film depends strongly on the sputter conditions,[23–27] these also influence the mechanical and thermal properties of the capping layer. At elevated temperatures, elastic stress due to the different thermal expansion coefficients of the organic and the aluminum oxide films is expected to evolve.

We performed measurements to characterize the effects of capping layer thickness, stoichiometry, and heating rate on the stability of these hybrid samples. The long-term stability of these samples at temperatures far above the desorption temperature of the DIP film was also investigated.

To obtain a picture as comprehensive as possible, we used a combination of x-ray diffraction techniques, thermal desorption spectroscopy, atomic force microscopy, transmission electron microscopy, and optical microscopy.

The paper is organized as follows: In Sec. II we describe the experimental setup and procedures. Section III presents our results on the structure and morphology of as-grown DIP films capped with aluminum oxide layers and with particular emphasis on their thermal stability. In Sec. IV, we discuss the results and discuss a possible breakdown scenario of the samples. Section V concludes this work with a brief summary.

II. EXPERIMENTAL

A. Preparation of organic films

Organic films of DIP were prepared on silicon wafers by organic molecular beam deposition[28,29] (with thicknesses ranging from 100 to 1000 Å). The structure and electrical properties of DIP films have been studied extensively in the past.[20,21,30]

After standard cleaning procedures, the substrates were transferred from a load lock into the preparation chamber where a base pressure from 10^{-11} to 10^{-10} mbar could be attained. Before the DIP growth, the substrates were outgased at temperatures between 650 and 700 °C for about 12 h. DIP was evaporated from home-built Knudsen cells, and the film thicknesses were determined with a quartz crystal microbalance. The pressures during deposition were in the range of 10^{-10} to 10^{-9} mbar. DIP films were prepared on Si(100) wafers with different oxide layer thicknesses (15–4000 Å). The growth rate was ≈5 Å/min, and the substrate temperature during growth was kept at 145 °C.

After preparation of the organic films, we used in situ atomic force microscopy (AFM) and x-ray diffraction methods to characterize the surface and the structure of the as-grown samples.

B. Preparation of aluminum oxide capping layers

The aluminum oxide layers (thickness from 166 to 5938 Å) were deposited on the organic films by high-frequency (HF)-magnetron sputtering in a separate chamber. To avoid oxidation of the underlying organic film, we used pure argon as sputter gas (argon partial pressure 2.6–2.8 × 10^{-3} mbar). Regarding the oxygen content, this leads to an under-stoichiometric target after some sputter cycles which had been overcome by regenerating the target after each deposition in an oxygen/argon atmosphere [$p(\mathrm{Ar}) \approx 5 \times 10^{-3}$ mbar, $p(\mathrm{O_2}) \approx 2 \times 10^{-3}$ mbar]. The base pressure of the chamber was 3 × 10^{-7} mbar, the deposition rate was about 7 Å / min, and the substrate temperature was kept at –10 °C.

C. Experimental methods

Different experimental techniques were used to investigate the properties of the capped and of the uncapped organic films.

X-ray diffraction techniques are particularly powerful for destructive-free investigation of the structure of buried interfaces. X-ray reflectivity (XRR), grazing incidence x-ray diffraction (GIXD), and diffuse x-ray scattering were used to determine the structural properties of the capped and uncapped organic films. From x-ray reflectivity measurements, we determined the electron density profile $\rho(z)$, and from the out-of-plane DIP Bragg peaks, we determined the lattice parameter of the organic film structure and the coherent film thickness, respectively.

We used these x-ray diffraction techniques in situ during the heating process to study possible diffusion and structural changes. The integrated intensity of the DIP Bragg reflection was used as a measure of the number of ordered molecules in the organic film. GIXD measurements supply us with information about the in-plane structure of the organic film and its lateral expansion during heating. The x-ray diffraction measurements were performed at the synchrotron facility ANKA at the Forschungszentrum Karlsruhe (Germany) and at laboratory x-ray sources at the Max-Planck-Institut für Metallforschung (MPI-MF) in Stuttgart (Germany).

For studies of the thermal stability of the capped organic films, we used thermal desorption spectroscopy (TDS). In the TDS experiments, the quadrupole mass

spectrometer is tuned to the mass of DIP molecules (400 amu), and the signal is recorded as a function of time, while the temperature is ramped at a constant rate. We studied the influence of different heating rates and different capping layer thicknesses on the thermal stability of the system. To guarantee capping of the entire organic film and to prevent edge effects, we used shadow masks for the organic film preparation.

AFM was used to study the surface morphology of the capped and uncapped organic films, and transmission electron microscopy (TEM) was used to investigate the insulator-organic interface. The preparation of cross-sectional TEM specimens is rather difficult for organic-inorganic film structures. Fortunately, the procedure, which had already been applied successfully to Au on DIP,[31] could also be applied to our system. The TEM measurements were performed with a Philips CM200 operated at 200 keV.

For the determination of the stoichiometry of the aluminum oxide layers, we used Rutherford backscattering spectroscopy (RBS). The measurements were carried out with He^+ ions of 1 MeV at the Dynamitron in Stuttgart. The RBS-chamber had an IBM-geometry (i.e., the detector was located at a $\theta = 165°$ scattering angle in the same plane as the beam and the normal to the sample) with a detector resolution of 14 keV full width at half-maximum (FWHM). The data were analyzed with the software RUMP.

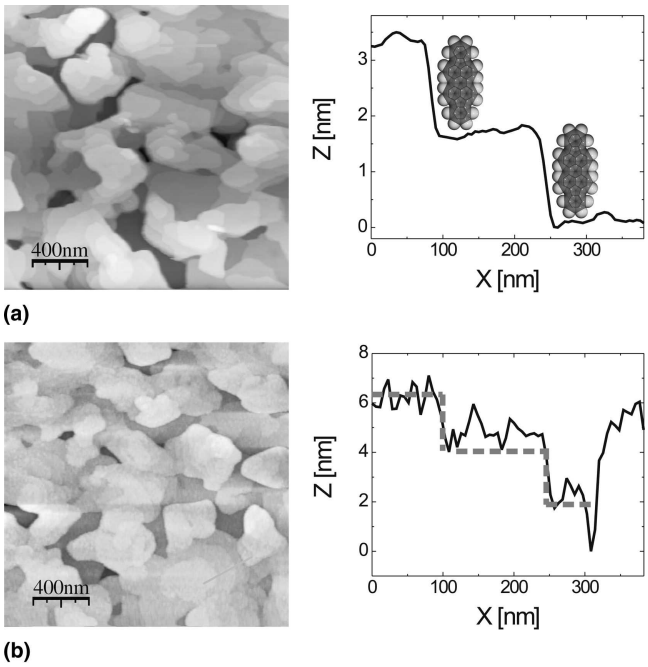

FIG. 1. Contact AFM image of a DIP sample (a) before and (b) after deposition of the aluminum oxide layer. The aluminum oxide layer exhibits a grainy morphology covering the terraced DIP structure.

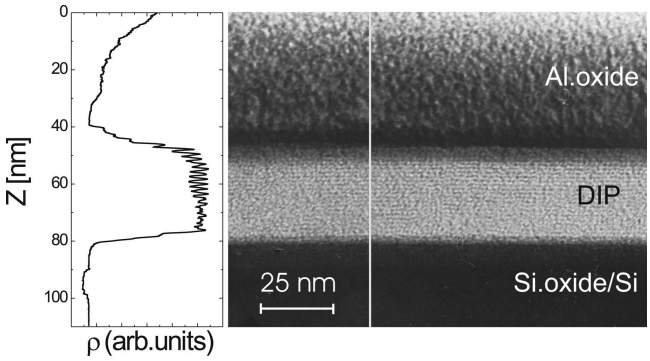

FIG. 2. TEM image showing a well-defined heterostructure of aluminum oxide on DIP/SiO_2. The laterally averaged image also shows the individual layers of DIP.

III. RESULTS

A. Characterization of capped DIP films under ambient conditions

1. Surface morphology

The structure and morphology of DIP films on silicon oxide have been described in detail elsewhere.[21,30] Briefly, they exhibit large flat terraces with a step height of ≈16.5 Å with the molecules standing essentially upright on the surface. The films can be prepared with a very high crystalline order.

A comparison between contact AFM images before and after the aluminum oxide deposition is shown in Fig. 1. After the aluminum oxide is deposited on top of DIP, the surface morphology of the DIP film can still be recognized. A closer look on the morphology of the aluminum oxide layer shows that the DIP surface is covered with a layer of small "grains" of aluminum oxide, which still reflects the main topographic features of the underlying organic film (terraces).

2. Multilayer structure of aluminum oxide on DIP

In Fig. 2, the TEM image of a typical sample shows the resulting heterostructure. Within the organic film, even individual molecular layers of DIP could be resolved. The density profile of this sample is shown by a laterally averaged image (see left panel in Fig. 2). Here, the periodic arrangement of the DIP lattice planes and the interfaces of the organic film with the substrate (silicon oxide) and the aluminum oxide capping layer can be seen. Note that the seemingly decreasing density of the aluminum oxide layer below 20 nm comes from the specimen preparation and is not real. Considering the DIP islands with their large flat terraces, their interface with the aluminum oxide capping layer was dominated by the DIP film roughness (aluminum oxide films prepared on bare silicon oxide exhibited low roughness). Nevertheless, the aluminum oxide/DIP interface was very well-defined and only limited interdiffusion could

be observed. The aluminum oxide layer exhibited a roughness of 40 Å.

The top curves in Figs. 3(a) and 3(b) show the x-ray reflectivity data of a DIP sample before and after the deposition of aluminum oxide (~1212 Å). The pronounced thickness oscillations (Kiessig interferences), which could be observed before and after the sputtering process (the low frequency oscillations coming from the DIP film and the high frequency oscillations coming from the aluminum oxide layer) indicated that the interfaces were still well defined. Comparing the Laue oscillations around the DIP Bragg peak the coherent thickness decreased from 368 Å before to 325 Å after the sputtering process. Therefore, the structural order of the first layers of the organic film was slightly compromised by the aluminum oxide deposition. For different samples prepared at lower sputtering powers (65 W instead of 150 W), no significant changes could be observed.

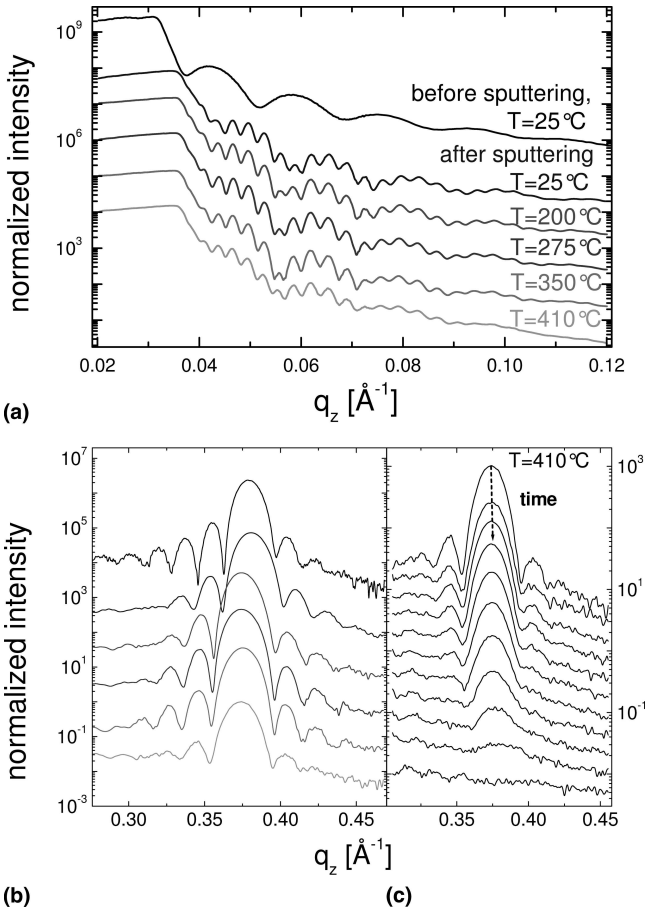

FIG. 3. Typical x-ray reflectivity scans of capped DIP films for different temperatures. (a) The reflectivity curves to a q_z value of 0.12 are displayed. (b) The DIP Bragg reflection is displayed for temperatures ranging from 25 to 410 °C [same order as in (a)]. At 410 °C the DIP Bragg peak disappears gradually. The different curves were taken approximately every 5 min (c). The different curves are scaled for clarity.

At higher scattering angles (i.e., in the Bragg regime), no signature for crystalline aluminum oxide was observed showing that the film was completely amorphous which was also confirmed by complementary TEM measurements.

3. Stoichiometry of the aluminum oxide layers

The stoichiometry of the aluminum oxide layer and incorporation of Ar in the capping layer could play a crucial role in the deterioration by crack formation at elevated temperatures. Cavities filled with Ar in the aluminum oxide film may influence the mechanical properties of the capping layer.[32–34] Therefore, the stoichiometry and the Ar content of the aluminum oxide films were determined by RBS.[35]

The Al/O ratio of our aluminum oxide samples ranged between 0.63 and 0.91 and thus from oxygen rich to metal rich films. The Ar content was found between 0.59 and 4.00 at.% depending on the preparation conditions.

B. Thermal stability—Desorption

After characterizing the as-grown samples we studied the thermal stability of capped DIP films. To investigate their overall thermal stability we measured TDS spectra of uncapped and capped DIP films (Fig. 4).

The uncapped DIP film had a well-defined peak around 190 °C, which we referred to as "bulk" desorption, while the desorption peaks for the capped DIP films were shifted to higher temperatures and exhibited a pronounced sub-structure. The capped films in Fig. 4 were heated with 30 °C/min and 10 °C/min, respectively. At lower heating rates, the center of mass of the TDS spectrum was shifted to higher temperatures. We consider the sharp peaks in the spectra of capped films to originate from individual desorption channels such as small

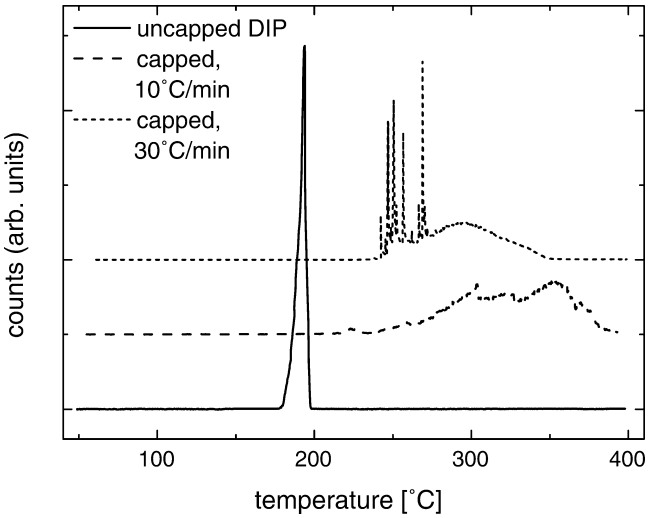

FIG. 4. TDS data of an uncapped versus capped DIP films for different heating rates.

cracks. These cracks or defects give rise to a limited local desorption of the underlying organic film but do not lead to the desorption of the entire film.

C. Thermal stability—Structure

1. Specular reflectivity—Interface structure

To obtain structural information of the system during the heating process, we performed in situ x-ray diffraction experiments. Figure 3 shows the specular reflectivity and the Bragg peak at different intermediate temperatures (the mean heating rate was about 0.75 °C/min) for a typical DIP film capped with an aluminum oxide layer (sample 8, see below). The Kiessig fringes in panel (a) show the different contributions from the DIP film (359.4 Å) with its low-frequency oscillations modulated by the contributions from the aluminum oxide film (1212 Å) high-frequency oscillations. They change only slightly with increasing temperature indicating that the interfaces do not change significantly upon heating. At around 410 °C, the thickness oscillations become less pronounced due to increasing roughness. In panel (b), the first order Bragg reflection of DIP is displayed as a function of temperature. Apart from the thermal expansion which shifts the peak to smaller q_z values no substantial changes can be observed. At 410 °C, however, the Bragg intensity decreases rapidly [Fig. 3(c)]. At this constant temperature, the Bragg peaks were monitored every 5 min starting from the upper curve (data are offset for clarity). Besides the decrease in intensity of the DIP Bragg peak and a small shift to higher q_z values, the Laue oscillations disappear, indicating that the coherence of the crystalline film is gradually reduced. The Bragg intensity eventually disappears at $T = 410$ °C.

From least-square fitting of the reflectivity curves by the Parratt-formalism, information about the temperature dependence of the electron density profile was obtained. Table I summarizes the results for the aluminum oxide and for the DIP layer. For this specific sample, the electron density of aluminum oxide remained nearly constant upon heating while the electron density for the DIP film decreased up to 410 °C, possibly due to thermal expansion.

To summarize, from the observations of the temperature-dependent reflectivity curves including the DIP Bragg reflection, we may conclude that the overall heterostructure remained essentially unchanged during heating. Aluminum oxide did not penetrate significantly into the DIP film and the crystalline structure of the organic film was not affected up to a certain, rather high temperature, which was specific for each sample (see below).

TABLE I. Results of least-square fitting to the Parratt formalism. Here, only the electron density ($\times 10^{-5}$ el/Å^3), the thickness (Å) and the roughness (Å) of the aluminum oxide and DIP films are displayed.

T (°C)	ρ_{Alox}	L_{Alox}	σ_{Alox}	ρ_{DIP}	L_{DIP}	σ_{DIP}
25	0.943	1212.4	33.4	0.396	359.4	27.8
200	0.957	1210.9	34.6	0.320	359.6	30.5
275	0.963	1210.0	34.8	0.306	362.1	30.8
350	0.962	1208.8	36.8	0.271	359.7	32.2
410	0.959	1204.9	38.0	0.276	363.6	36.9

2. Off-specular scattering—Disorder

X-ray scattering experiments contain information on the statistical properties of surfaces or interfaces, i.e., the lateral length of surface morphologies (via transverse rocking scans) and the correlations between buried interfaces (via longitudinal off-specular scans). Diffuse scattering data were detected in two different geometries, namely transverse ("rocking") scans and longitudinal ("offset") scans. Figure 5(a) illustrates the different scans in reciprocal space.

The inset of Fig. 5(b) shows a transverse scan of

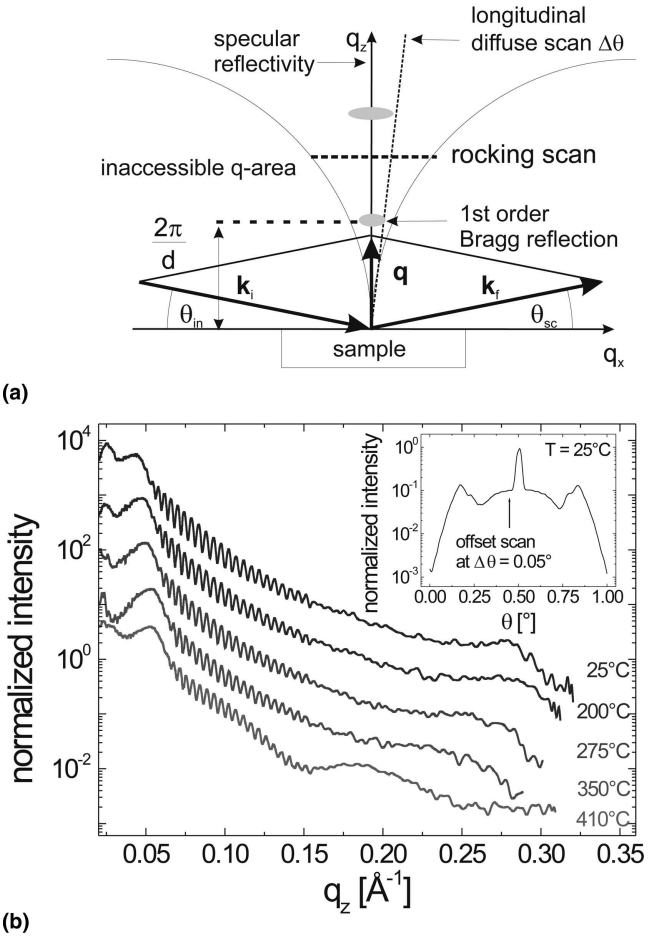

FIG. 5. (a) Scans in reciprocal space with representation of specular reflectivity, transverse rocking and longitudinal offset scans. (b) Longitudinal offset scans of Al_2O_3/DIP ($\Delta\theta = 0.05°$) for different temperature steps scaled for better visibility. The inset shows a room temperature transverse rocking scan taken around $\theta = 0.5°$ ($2\theta = 1.0° = \text{const.}$, $\lambda = 1.078$ Å).

aluminum oxide on DIP at room temperature around $\theta = 0.5°$ ($2\theta = 1.0° = \text{const.}$, $\lambda = 1.078$ Å). The rocking curve consists of the narrow specular scattering contributions of the DIP film and the broader scattering contribution of the disordered aluminum oxide film.

The longitudinal offset-scans in Fig. 5(b) were taken at an offset angle of $\Delta\theta = 0.05°$ for each temperature step. These longitudinal diffuse scans were used to subtract diffuse scattering from the specular scattering. Also, they allow for the determination of the aluminum oxide layer thickness [high-frequency oscillations in Fig. 5(b)] independent from the specular x-ray reflectivity data due to the relatively broad rocking curve of the aluminum oxide layer ($\gg 0.05°$). For the oscillations corresponding to the aluminum oxide film, no significant changes could be observed up to 410 °C. Furthermore, the diffuse scattering from a relatively thin disordered layer (low frequency oscillation), which increases with temperature up to about 50 Å in thickness at 410 °C, is observed. This thin layer neither corresponds to the aluminum oxide layer (1212 Å) nor does it correspond to the silicon oxide layer, which has a thickness around 14 Å. We may speculate that this disordered layer may originate from diffusion of the sputtered material already upon deposition into the top few layers of DIP and which further diffuses into the organic film with increasing temperature, thus destroying the high structural order of the top DIP layers. A similar effect was observed for the deposition of metals on organics.[36,37]

3. Bragg intensities—Crystallinity

In addition to the position of the Bragg reflection, which gives the out-of-plane lattice parameter, the integrated intensity, which gives the degree of order in the film, was evaluated. Its temperature dependence gives the thermal disordering of the DIP film. It was calculated by multiplying the area under the background-corrected Bragg peak with the rocking width. The integrated Bragg intensity was used to compare the influence of different experimental conditions and material properties (capping layer thickness, stoichiometry and heating rate) on the stability of the organic film (Fig. 6). The specifications of these samples are given in Table II.

In the following by the term "breakdown temperature", we will mean the temperature at which the integrated intensity starts to drop significantly. This allows comparison of the thermal stability of samples with different film thicknesses, stoichiometries, etc. Comparing the integrated intensities of these samples, we conclude that in accordance with TDS data, higher heating rates shift the breakdown temperature to smaller values (sample 3). Furthermore, thicker capping layers (sample 6) are more stable than thin capping layers (sample 5), and the metal-rich oxide layers (sample 4) show the tendency to break down at lower temperatures. (Note, for samples 2, 3, and 4, the stoichiometries were not determined, but from comparison with RBS measurements on different samples sputtered under comparable conditions, a qualitative estimate is possible. In particular, for sample 4, a higher metallic content can be concluded. The limited stability of metal-rich capping layers could be seen in a series with purely metallic "capping" layers (sample 7), which penetrate into the organic film at elevated temperatures and destroy the structural order of the organic film.[36,37]

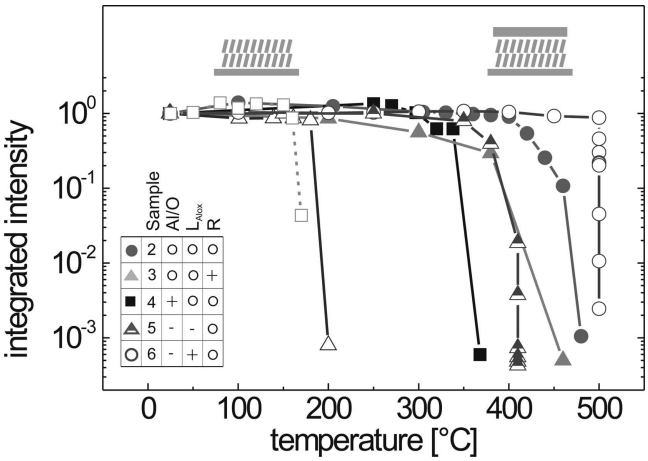

FIG. 6. Comparison of the integrated Bragg intensity of different samples. Sample 1 (open triangle) had no capping layer, samples 2–6 had an aluminum oxide capping layer but different sample specifications or heating rates (see Table II). Sample 7 (open square) had a gold film instead of an aluminum oxide layer on top of DIP.[36]

TABLE II. Sample parameters, i.e., thickness and stoichiometry (Al:O ratio, Ar content) of the aluminum oxide capping layer, DIP film thickness, and the mean heating rate.

Sample	L_{cap} (Å)	L_{DIP} (Å)	Al:O	Ar (at.%)	$R_{heating}$ (°C/min)	$T_{breakdown}$ (°C)
1	⋯	773	⋯	⋯	0.89	200
2	607	1002	(0.66)[a]	(–)[a]	0.49	480
3	618	773	(0.66)[a]	(–)[a]	2.66	460
4	662	479	(>0.66)[a]	(–)[a]	0.33	360
5	166	334	0.606	0.75	0.56	410
6	5938	402	0.63	0.59	0.58	500
7	135[b]	385	⋯	⋯	⋯	160
8	1212	360	0.733	0.40	0.75	410
9	520	450	0.602	0.37	0.37	410

[a]Values not known/estimated.
[b]Gold capping layer.[36]

4. Lattice parameters

The out-of-plane lattice parameter *c* (see Fig. 7) could be determined from x-ray reflectivity measurements for a capped (sample 5) and an uncapped DIP film (sample 1) as a function of temperature. Up to temperatures of around 200 °C, the lattice parameters *c* increased linearly with temperature for both uncapped and capped

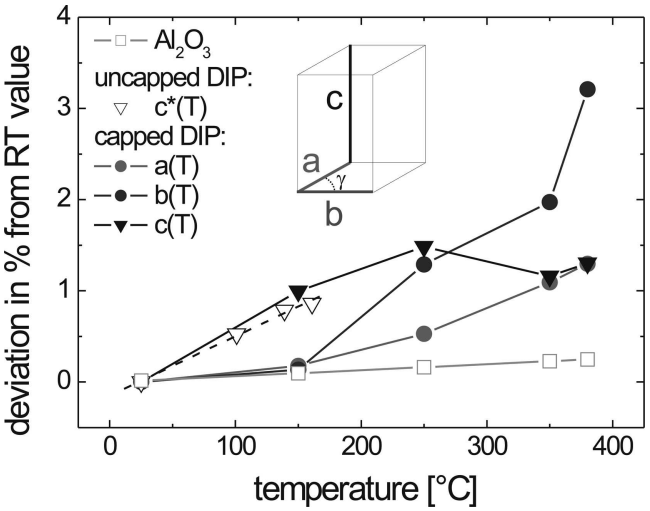

FIG. 7. Relative change of the lattice parameters of a capped DIP film on silicon oxide as a function of temperature. The room temperature values are $a = 8.55$ Å, $b = 7.05$ Å, and $c = 16.57$ Å. For comparison, the temperature dependence of the lattice parameter c^* of an uncapped DIP film and the relative thermal expansion of aluminum oxide are plotted.

films and a thermal expansion coefficient of $\alpha_{\|}^{*} = 65.0 \times 10^{-6}\ K^{-1}$ and $\alpha_{\|} = 66.6 \times 10^{-6}\ K^{-1}$, respectively, could be extracted. Above 200 °C, the thermal behavior of the capped film differed strongly from a linear behavior. This might be explained by structural changes and stresses in the film or at the film interfaces.

From radial scans of DIP on silicon oxide (the DIP domains are randomly oriented in-plane) the three GIXD reflections at $q_{\|} = 1.155\ Å^{-1}$, $q_{\|} = 1.469\ Å^{-1}$, and $q_{\|} = 1.717\ Å^{-1}$ were measured as a function of temperature. According to the DIP unit cell proposed by Dürr et al.[38] these reflections correspond to the (11), (20), and (21) reflections, respectively. At room temperature, the following parameters for the capped DIP film could be obtained: $a = 8.55$ Å, $b = 7.05$ Å, $c = 16.57$ Å, and $\gamma = 89.7°$. The temperature dependent evolution of *a, b,* and *c* is displayed in Fig. 7 (γ remained constant within 0.3°).

The in-plane lattice parameters *a* and *b* do not show linear behavior. Up to 150 °C, the thermal behavior of *a* and *b* is comparable to the thermal expansion of sputtered aluminum oxide films, for which values of $\alpha = 6.5 \times 10^{-6}\ K^{-1}$ are reported.[18] Above 150 °C, the DIP lattice parameters *a* and *b* show a much stronger increase than aluminum oxide and if approximated to a linear behavior, the thermal expansion coefficient of *a* and *b* is around $48.8 \times 10^{-6}\ K^{-1}$ and $118.2 \times 10^{-6}\ K^{-1}$, respectively. Regarding the effect of thermal expansion, compressive and tensile stresses on the position of a Bragg reflection (shift to lower, higher and lower *q* values, respectively) the complex thermal behavior of the DIP lattice parameters *a, b,* and *c* can be understood in terms of thermal expansion and the formation and relaxation of thermally induced stresses in the organic film and at the interface to the aluminum oxide layer.

Furthermore, the typical pyramidal structure of DIP films leads to lateral stresses acting on the aluminum oxide, which gradually decrease from layer *i* to layer *i* + 1, and it leads to vertical stresses acting on the aluminum oxide, which gradually increase from layer *i* to layer *i* + 1, as illustrated in Fig. 8. Inhomogeneities in the aluminum oxide layer such as regions with a higher content of trapped Ar or regions with a different stoichiometry may also enhance or relax the thermal stresses in the aluminum oxide film.

The large mismatch in the thermal expansion of organic and aluminum oxide film (around one order of magnitude) enhances the thermally induced stresses, which at some point can no longer be accomodated, thus leading to fracture of the capping layer.

D. Long-term stability

To evaluate time-dependent effects upon heating, one sample was kept at an intermediate temperature (300 °C) while recording the DIP Bragg peak with its Laue oscillations for more than 300 h (see Fig. 9).

The results clearly show that the integrated intensity decreases with time (to 50% of its initial value after 100 h) while the coherent thickness of the organic film remains unchanged over the whole period of time (within 5 Å). This supports the TDS data, which suggested that DIP already desorbs in a temperature range between the desorption temperature of the uncapped film (190 °C) and the breakdown temperature of the capped film. The desorption of DIP is largely prevented by the aluminum oxide film, but pinholes and cracks in the capping layer

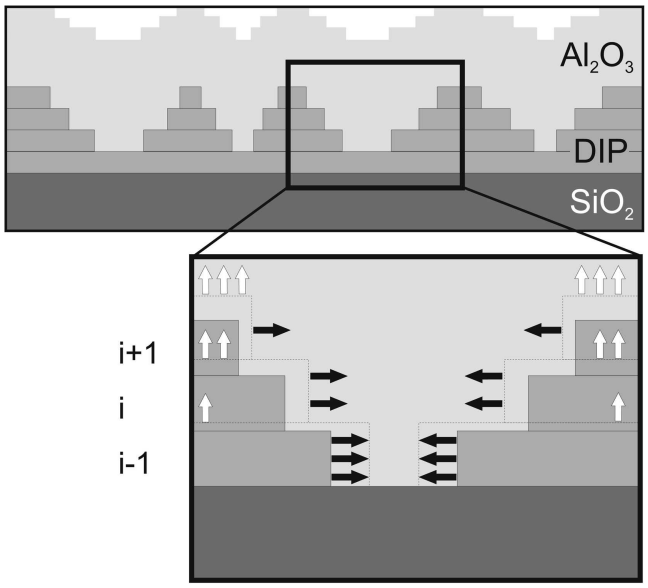

FIG. 8. Schematic representation of the aluminum oxide/DIP interface.

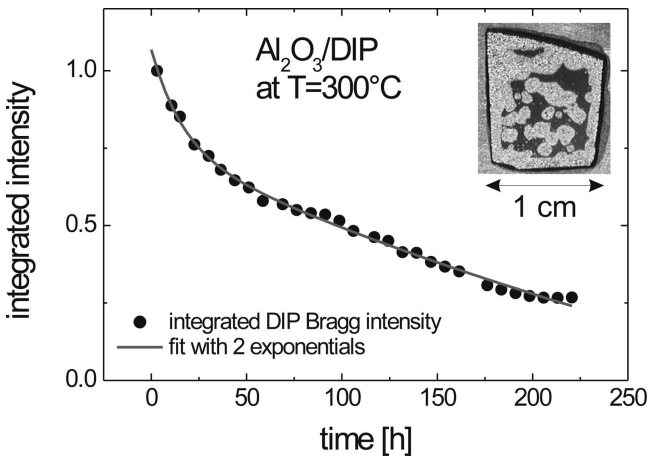

FIG. 9. Time-dependence of the Bragg intensity of a capped DIP film kept at 300 °C. The decrease of the Bragg intensity can be fitted to two exponentials having a short-term and a long-term contribution. After 100 h, it has decreased to about half the value of the starting intensity. The DIP film had a thickness of about 700 Å and an aluminum oxide thickness of about 600 Å.

lead to a finite desorption rate, and thus the desorption of DIP is kinetically limited. The decrease of the Bragg intensity can be fitted to two exponentials with a short-term (time constant: 16 h) and a long-term (time constant: 517 h) contribution. Because the coherent thickness remained constant during the heating process, the observed decrease of the integrated Bragg intensity at 300 °C with time is related to desorption of the organic film from areas located in the proximity of the defects in the capping layer—for example microcracks or holes—and to desorption from uncapped side-edges of the sample. It is not desorbing "layer by layer" in a laterally homogeneous way, as would be possible for desorption from uncapped films.

The photograph in Fig. 9 (inset) shows the sample after 400 h at 300 °C. We note that the DIP film covered the entire substrate which led to desorption from the edges of the sample. We attribute the bright parts of the sample to those where DIP had already desorbed. Obviously, a non-negligible contribution came from desorption at the edges. However, desorption from the middle of the sample could be observed. The circular shape of these areas might come from the desorption of the molecules through defects in the capping layer (represented by the short term contribution of the Bragg intensities) and succesive diffusion to these defects (long term contribution). The histogram of the color distribution (not shown) of the sample suggests that the brighter parts, and therefore the parts where DIP had already desorbed, cover 72.5% of the sample surface. This means that 27.5% of the DIP film is still on the sample which is consistent with the long-term measurements where about 20% of the initial integrated intensity were left after 250 h.

IV. DISCUSSION

The characterization of the as-prepared samples has shown that the aluminum oxide layer exhibits a grainy morphology, covering the terraced DIP surface. Details of the film structure depend on the specific preparation conditions. The stoichiometry and the Ar content of these capping layers may also differ accordingly and therefore, also the mechanical and thermal properties.

X-ray diffraction and TEM measurements have shown that the aluminum oxide/DIP interface shows only limited penetration even after heating to 400 °C. The thermal stability of the samples depends strongly on the heating rate (lower heating rates lead to higher breakdown temperatures), which was confirmed by both TDS and x-ray reflectivity measurements. Thicker aluminum oxide capping layers were more effective in producing a higher thermal stability (at least up to thicknesses of 60 nm), which could be caused by a better compensation of defects or a better relaxation of stresses compared to thin capping layers. Aluminum oxide films with a higher metallic content were found to be less stable. The higher mobility of metal-rich capping layers thus might have facilitated crack and defect formation at elevated temperatures.

During the heating process, the organic film of DIP remained highly ordered up to temperatures more than 200 °C above its (uncapped) desorption temperature. From TDS measurements, we know that desorption of the organic molecules starts about 50 °C above the desorption temperature of uncapped films probably due to local defects in the capping layer. This is supported by long-term XRR measurements, which show that the number of ordered molecules decreases with time at a fixed temperature ($T > 190$ °C). As the coherent thickness of the DIP film remained constant during the heating process the desorption process is apparently hindered locally.

The origin of these defects in the capping layer might be thermally induced since there was no desorption found in a 50 °C temperature range above the desorption temperature of uncapped films. GIXD measurements have shown that the lateral thermal expansion of the organic film is constrained up to ~150 °C and then suddenly increases to a value about one order of magnitude larger than the thermal expansion of the aluminum oxide capping layer.

It is not easy to identify a simple microscopic mechanism driving the eventual breakdown. Nevertheless, certain scenarios can be discussed. One possible mechanism of the breakdown scenario, which we could derive from our results, is related to the large mismatch in the thermal expansion at the Alox/DIP interface (see Fig. 7). The optical micrograph in Fig. 10(a) shows a sample for which the DIP was deposited with a shadow mask and

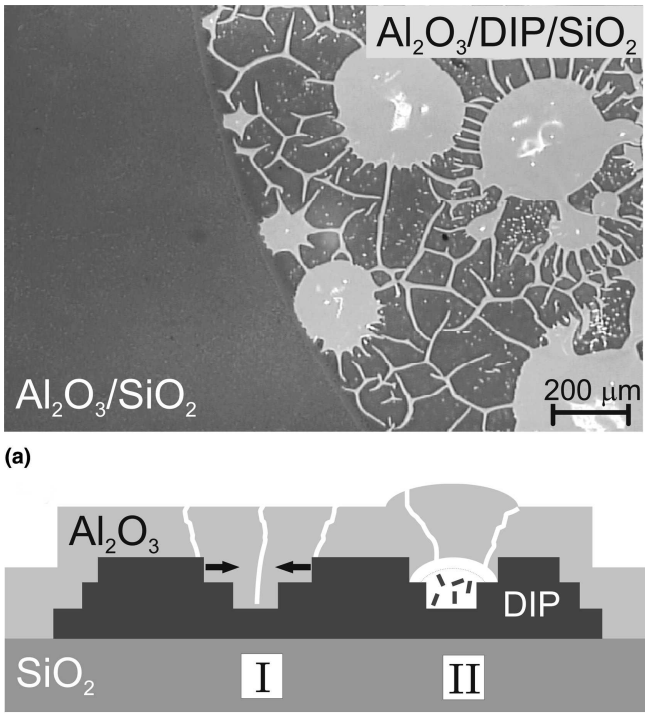

FIG. 10. Optical micrograph of a heated Alox/DIP/SiO_2 sample where the DIP film was only deposited in the middle of the sample. An extended network of cracks can be observed, which is only limited to the region where the organic film was located underneath.

afterwards aluminum oxide was deposited without mask. Note, that the cracks were only located on the Alox/DIP/SiO_2 and not on the Alox/SiO_2.

The terrace structure of DIP films leads to lateral stresses acting on the aluminum oxide, which increase with the DIP layer number (starting from the first monolayer); this leads to vertical stresses acting on the aluminum oxide, which increase with the DIP layer number. The large mismatch between the thermal expansion of the aluminum oxide and the DIP films and possible relaxations of stresses finally lead to a strain-induced crack formation in the aluminum oxide layer when the temperature is increased. These thermally induced defects allow the desorption of DIP molecules located under these defects. In a second step, even molecules from well-capped areas diffuse to the defects to desorb from there. This scenario (I) would assume a failure of the aluminum oxide capping layer due to the thermomechanical mismatch between the different materials.

Nevertheless, a second scenario (II) could also be possible, which is based on a secondary failure of the capping layer. During the aluminum oxide sputtering, some voids may have formed between the aluminum oxide and the DIP film, which allow a local desorption of DIP when heated above the desorption temperature. The partial pressure in the cavities might increase and expand the "bubbles", which increases stress in the aluminum oxide layer and possible crack formation and desorption, accordingly.

V. SUMMARY AND CONCLUSIONS

We performed a detailed study of the parameters, which influence the thermal stability of organic films of DIP capped by an aluminum oxide layer. The strongly enhanced thermal stability is due to the aluminum oxide layer serving as an almost perfect "lid" for the DIP. The crucial question is what is limiting the thermal stability of aluminum oxide and what is leading to the eventual breakdown.

From TDS and x-ray diffraction measurements it turned out that the stability can be further enhanced by using thicker aluminum oxide layers. The heating rate also plays a role for relaxation processes which compete with the thermally induced stress at the aluminum oxide/DIP interface. Since the thermomechanical properties of the aluminum oxide layers change with its composition the stoichiometry of the capping layer plays a major role in the breakdown scenario. From our results, we conclude that thicker capping layers and low heating rates are more favorable for the high-temperature stability and metal-rich capping layers tend to break down at lower temperatures compared to stoichiometric (Al_2O_3) capping layers.

For the eventual breakdown of the capped film structure, we presented a possible scenario based on the failure of the aluminum oxide capping layer due to thermally induced crack formation and subsequent desorption of the organic molecules.

We believe that the use of aluminum oxide layers as an encapsulation material has significant potential for the application in organic devices. Capping layers do not only prevent molecules from the organic layer to desorb at elevated temperatures, but they also promise to prevent ambient gases from penetration into the organic semiconductor film. This is not only valid for the specific molecule of DIP but was also shown to work for more popular molecules such as pentacene.[39] One might therefore also think about using organic semiconductor molecules, which have desorption temperatures so far considered too low for practical application.[40] Besides the practical use of a cappig layer, we point out that a capping layer allows to study material properties beyond the desorption temperature of the specific molecule and thus to study the behavior under conditions otherwise inaccessible.

ACKNOWLEDGMENTS

We acknowledge support by the Deutsche Forschungsgemeinschaft (DFG) within the Focus Programme on organic field effect transistors and support from the Engineering and Physical Sciences Research Council

(EPSRC). We are grateful to the FZ Karlsruhe and the ANKA management for their generous support and H. Paulus and W. Bolse from the Institut für Strahlenphysik for the RBS measurements.

REFERENCES

1. *Physics of Organic Semiconductors,* edited by W. Brütting (Wiley-VCH, Weinheim, Germany, 2005).
2. G. Horowitz: Organic thin film transistors: From theory to real devices. *J. Mater. Res.* **19,** 1946 (2004).
3. S.R. Forrest: The path to ubiquitous and low-cost organic electronic appliances on plastic. *Nature* **428,** 911 (2004).
4. C.D. Dimitrakopoulos and P.R.L. Malenfant: Organic thin film transistors for large area electronics. *Adv. Mater.* **14,** 99 (2002).
5. A. Dodabalapur, J. Laquindanum, H.E. Katz, and Z. Bao: Complementary circuits with organic transistors. *Appl. Phys. Lett.* **69,** 4227 (1996).
6. S. Scheinert and W. Schliefke: Analyzes of field-effect devices based on poly(3-octylthiophene). *Synth. Met.* **139,** 501 (2003).
7. R. Ye, M. Baba, K. Suzuki, Y. Ohishi, and K. Mori: Effects of O_2 and H_2O on electrical characteristics of pentacene thin film transistors. *Thin Solid Films* **464–465,** 437 (2004).
8. Ch. Pannemann, T. Diekmann, and U. Hilleringmann: Degradation of organic field-effect transistors made of pentacene. *J. Mater. Res.* **19,** 1999 (2004).
9. J.R. Sheats, H. Antoniadis, M. Hueschen, W. Leonard, J. Miller, R. Moon, D. Roitman, and A. Stocking: Organic electroluminescent devices. *Science* **273,** 884 (1996).
10. X. Zhou, J. He, L.S. Liao, M. Lu, X.M. Ding, X.Y. Hou, X.M. Zhang, X.Q. He, and S.T. Lee: Real-time observation of temperature rise and thermal breakdown processes in organic LEDs using an IR imaging and analysis system. *Adv. Mater.* **12,** 265 (2000).
11. N.M. Paulo dos Anjos, H. Aziz, N-X. Hu, and Z.D. Popovic: Temperature dependence of electroluminescence degradation in organic light-emitting devices without and with a copper phthalocyanine buffer layer. *Org. Electron.* **3,** 9 (2002).
12. F. Schreiber, M.C. Gerstenberg, H. Dosch, and G. Scoles: Melting point enhancement of a self-assembled monolayer induced by a van der Waals bound capping layer. *Langmuir* **19,** 10004 (2003).
13. P. Fenter, F. Schreiber, V. Bulović, and S.R. Forrest: Thermally induced failure mechanisms of organic light emitting device structures probed by x-ray specular reflectivity. *Chem. Phys. Lett.* **277,** 521 (1997).
14. B. Krause, A.C. Dürr, F. Schreiber, H. Dosch, and O.H. Seeck: Thermal stability and partial dewetting of crystalline organic thin films: 3,4,9,10-perylenetetracarboxylic dianhydride on Ag(111). *J. Chem. Phys.* **119,** 3429 (2003).
15. K.M. Kim, B.J. Jang, W.S. Cho, and S.H. Ju: The property of encapsulation using thin film multi layer for application to organic light emitting device. *Curr. Appl. Phys.* **5,** 64 (2005).
16. G.H. Kim, J. Oh, Y.S. Yang, L-M. Do, and K.S. Suh: Lamination process encapsulation for longevity of plastic-based organic light-emitting devices. *Thin Solid Films* **467,** 1 (2004).
17. J.H. Lee, G.H. Kim, S.H. Kim, S.C. Lim, Y.S. Yang, J. Oh, J.H. Youk, J. Jang, and T. Zyung: The novel encapsulation method for organic thin-film transistors. *Curr. Appl. Phys.* **5,** 348 (2005).
18. R.G. Munro: Evaluated material properties for a sintered α-alumina. *J. Am. Ceram. Soc.* **80,** 1919 (1997).
19. W.H. Gitzen: *Alumina as a Ceramic Material* (The American Ceramic Society, Westerville, OH, 1997).
20. N. Karl: Charge-carrier mobility in organic molecular crystals, in *Organic Electronic Materials,* Springer Series in Materials Science, Vol. 41, edited by R. Farchioni and G. Grosso (Springer, Berlin, Germany, 2001), Chap. 3.
21. A.C. Dürr, F. Schreiber, M. Münch, N. Karl, B. Krause, V. Kruppa, and H. Dosch: High structural order in thin films of the organic semiconductor diindenoperylene. *Appl. Phys. Lett.* **81,** 2276 (2002).
22. S. Sellner, A. Gerlach, F. Schreiber, M. Kelsch, N. Kasper, H. Dosch, S. Meyer, J. Pflaum, M. Fischer, and B. Gompf: Strongly enhanced thermal stability of crystalline organic thin films induced by aluminum oxide capping layers. *Adv. Mater.* **16,** 1750 (2004).
23. C.S. Bhatia, G. Guthmiller, and A.M. Spool: Alumina films by sputter deposition with Ar/O_2: Preparation and characterization. *J. Vac. Sci. Technol. A* **7,** 1298 (1989).
24. R. Cueff, G. Baud, J.P. Besse, and M. Jacquet: Study of thin alumina coatings sputtered on polyethylene terephthalate films. *Thin Solid Films* **266,** 198 (1995).
25. K. Koski, J. Hölsä, and P. Juliet. Properties of aluminium oxide thin films deposited by reactive magnetron sputtering. *Thin Solid Films* **339,** 240 (1999).
26. J. Lee, S.S. Kim, and S. Im: Electrical properties of aluminum oxide films deposited on indium-tin-oxide glasses. *J. Vac. Sci. Technol. B* **21,** 953 (2003).
27. O. Zywitzki and G. Hoetzsch: Influence of coating parameters on the structure and properties of Al_2O_3 layers reactively deposited by means of pulsed magnetron sputtering. *Surf. Coat. Technol.* **86–87,** 640 (1996).
28. F. Schreiber: Organic molecular beam deposition: Growth studies beyond the first monolayer. *Phys. Status Solidi* **201,** 1037 (2004).
29. G. Witte and C. Wöll: Growth of aromatic molecules on solid substrates for applications in organic electronics. *J. Mater. Res.* **19,** 1889 (2004).
30. A.C. Dürr, F. Schreiber, K.A. Ritley, V. Kruppa, J. Krug, H. Dosch, and B. Struth: Rapid roughening in thin film growth of an organic semiconductor (diindenoperylene). *Phys. Rev. Lett.* **90,** 016104 (2003).
31. A.C. Dürr, F. Schreiber, M. Kelsch, and H. Dosch: Optimized preparation of cross sectional TEM specimens of organic thin films. *Ultramicroscopy* **98,** 51 (2003).
32. F.M. D'Heurle and J.M.E. Harper: Note on the origin of intrinsic stresses in thin films deposited via evaporation and sputtering. *Thin Solid Films* **171,** 81 (1989).
33. L. Parfitt, M. Goldiner, J.W. Jones, and G.S. Was: Residual stresses in amorphous alumina films synthesized by ion-beam-assisted deposition. *J. Appl. Phys.* **77,** 3029 (1995).
34. K. Koski, J. Hölsä, P. Juliet, Z.H. Wang, R. Aimo, and K. Pischow: Characterisation of aluminium oxide thin films deposited on polycarbonate substrates by reactive magnetron sputtering. *Mater. Sci. Eng. B* **65,** 94 (1999).
35. H. Paulus and W. Bolse (unpublished).
36. A.C. Dürr, F. Schreiber, M. Kelsch, H.D. Carstanjen, and H. Dosch: Morphology and thermal stability of metal contacts on crystalline organic thin films. *Adv. Mater.* **14,** 961 (2002).
37. M. Scharnberg, J. Hu, J. Kanzow, K. Rätzke, R. Adelung, F. Faupel, C. Pannemann, U. Hilleringmann, S. Meyer, and J. Pflaum: Radiotracer measurements as a sensitive tool for the detection of metal penetration in molecular-based organic electronics. *Appl. Phys. Lett.* **86,** 024104 (2005).
38. A.C. Dürr, N. Koch, M. Kelsch, A. Rühm, J. Ghijsen, R.L. Johnson, J-J. Pireaux, J. Schwartz, F. Schreiber, H. Dosch, and A. Kahn: Interplay between morphology, structure and electronic properties at diindenoperylene-gold interfaces. *Phys. Rev. B* **68,** 115428 (2003).
39. S. Meyer, S. Sellner, F. Schreiber, H. Dosch, G. Ulbricht, M. Fischer, B. Gompf, and J. Pflaum (unpublished).
40. J. Niemax and J. Pflaum (unpublished).